ChemPubSoc Europe

DOI: 10.1002/cctc.201601228

CHEMCATCHEM Full Papers

Effects of the Functionalization of the Ordered Mesoporous Carbon Support Surface on Iron Catalysts for the Fischer–Tropsch Synthesis of Lower Olefins

Martin Oschatz,*[a] Jan P. Hofmann,[b] Tom W. van Deelen,[a] Wouter S. Lamme,[a] Nynke A. Krans,[a] Emiel J. M. Hensen,[b] and Krijn P. de Jong*[a]

Ordered mesoporous carbon (CMK-3) with different surface modifications is applied as a support for Fe-based catalysts in the Fischer–Tropsch to olefins synthesis (FTO) with and without sodium and sulfur promoters. Different concentrations of functional groups do not affect the size (3–5 nm) of Fe particles in the fresh catalysts but iron (carbide) supported on N-enriched CMK-3 and a support with a lower concentration of functional groups show higher catalytic activity under industrially relevant FTO conditions (340 °C, 10 bar, $H_2/CO = 2$) compared to a support with an O-enriched surface. The addition of promoters leads to more noticeable enhancements of the catalytic activity (3–5 times higher) and the selectivity to C_2–C_4 olefins (≈2 times higher) than surface functionalization of the support. Nitrogen surface functionalization and removal of surface groups before impregnation and calcination, however, further increase the activity of the catalysts in the presence of promoters. The confinement of the Fe nanoparticles in the mesopores of CMK-3 restricts but does not fully prevent particle growth and, consequently, the decrease of activity under FTO conditions.

Introduction

C_2–C_4 olefins are crucial intermediates for the production of plastics and fine chemicals and in the fuel industry.[1,2] Conventionally, these components are produced mainly by the steam cracking of naphtha or fluid catalytic cracking of vacuum gas oil. As a result of the rapid depletion and volatile price of crude oil as well as environmental concerns, non-oil-based feedstocks for lower olefins production are increasingly required.[2] Particularly, the use of synthesis gas has attracted considerable attention in recent years.[3,4] Syngas is a mixture of CO and H_2 that can be derived from, for example, coal, natural gas, and biomass. It can be converted to C_2–C_4 olefins either through a methanol or dimethyl ether route[5,6] or directly by using bifunctional catalysts.[7,8] The direct hydrogenation of CO is known as the Fischer–Tropsch to olefins (FTO) process.[2,9]

Although Co[10,11] and Fe[12,13] are the commonly used Fischer–Tropsch metals, nanostructured iron (carbide) catalysts are applied in the high-temperature FTO process because of their low methane selectivity, high abundance, high water gas shift activity, and low cost.[2,14] Although numerous species (iron oxides, metallic iron, iron carbides, and their combinations) can play a role in the FTO process, it has been shown that iron carbides are the catalytically active phase.[15] Recently, it was foundthat especially the addition of a combination of Na and S promoters can suppress methane formation and increase the activity of FTO catalysts at the same time.[16,17]

Fe nanoparticles are often supported on porous inorganic substrates to avoid the rapid deactivation of the catalyst caused by sintering and mechanical breakdown.[18–20] Especially, nanostructured carbon materials have received considerable attention as supports for Fe-based FTO catalysts in recent years.[21–25] Their weak interaction with Fe species facilitates the formation of catalytically active iron carbide species and, therefore, high catalytic activity can be achieved.[9] The irreversible formation of nonreducible and hence inactive Fe species that may occur for silica and high-surface-area alumina is suppressed on carbonaceous supports. Moreover, carbon supports are highly versatile in terms of their textural and chemical properties, that is, their pore size, pore geometry, carbon nanostructure, and surface functionalization.[26,27]

[a] Dr. M. Oschatz, T. W. van Deelen, W. S. Lamme, N. A. Krans, Prof. Dr. K. P. de Jong
Group of Inorganic Chemistry and Catalysis
Debye Institute for Nanomaterials Science, Utrecht University
Universiteitsweg 99
3584 CG Utrecht (The Netherlands)
E-mail: M.Oschatz@uu.nl
K.P.deJong@uu.nl

[b] Dr. J. P. Hofmann, Prof. Dr. E. J. M. Hensen
Laboratory of Inorganic Materials Chemistry,
Department of Chemical Engineering and Chemistry
Eindhoven University of Technology
Groene Loper 5
5612 AE Eindhoven (The Netherlands)

Supporting information for this article can be found under: http://dx.doi.org/10.1002/cctc.201601228.

This manuscript is part of a Special Issue to celebrate the 50th annual meeting of the German Catalysis Society.

Recent studies have shown that the surface chemistry of carbon support materials plays a crucial role in Fe-based FTO catalysts. Lu et al. reported that N-enriched carbon nanotube (CNT) surfaces can enhance the reduction of iron oxides to catalytically active iron carbides and that they can increase the selectivity towards lower olefins because of their intrinsic basicity, which enhances dissociative CO adsorption and promotes the desorption of C_2–C_4 olefins. The anchoring effects and basicity of the N-doped CNTs also lead to the enhanced stability of the catalysts by preventing the loss of active species and basic sites during operation.[28] In several studies, Muhler and coworkers showed that N-functionalized CNTs provide a higher catalytic activity and stability than O-functionalized CNTs because of the more severe sintering of Fe particles deposited on the latter, which results from the higher thermal stability of N groups than O groups.[29–31]

Most of these studies were performed with CNTs or other highly graphitic materials as supports because of their well-defined surface chemistry and the numerous available studies on their surface functionalization.[28,32] However, especially in the presence of promoters, particle growth occurs for Fe particles on supports with a large external surface area.[33] The encapsulation of Fe into mesoporous carbon materials with a rather disordered carbon microstructure is one way to slow particle growth and to stabilize the catalytically active particles.[15] However, much less is known about the influence of the surface properties of such supports on the properties of FTO catalysts. Although it is known that the chemical surface properties of the support materials can have a strong influence on the efficiency of promoters,[15,20] the effect of surface functional groups on carbon supports in the presence of Na/S has not been investigated.

We apply an ordered mesoporous carbon, CMK-3,[34] after different surface functionalization treatments as a support for Fe-based FTO catalysts with and without Na and S as promoters. O-enriched CMK-3 is prepared by the heating of the parent material in air. N-functionalization is achieved by heating the O-enriched material in an ammonia flow. Large parts of the surface groups are removed by heating the parent material under N_2 flow. Although these treatments do not change the Fe particle size and dispersion significantly after impregnation and calcination, significant differences in the catalytic activities are observed as a function of the surface properties of CMK-3, especially in the presence of Na and S as promoters.

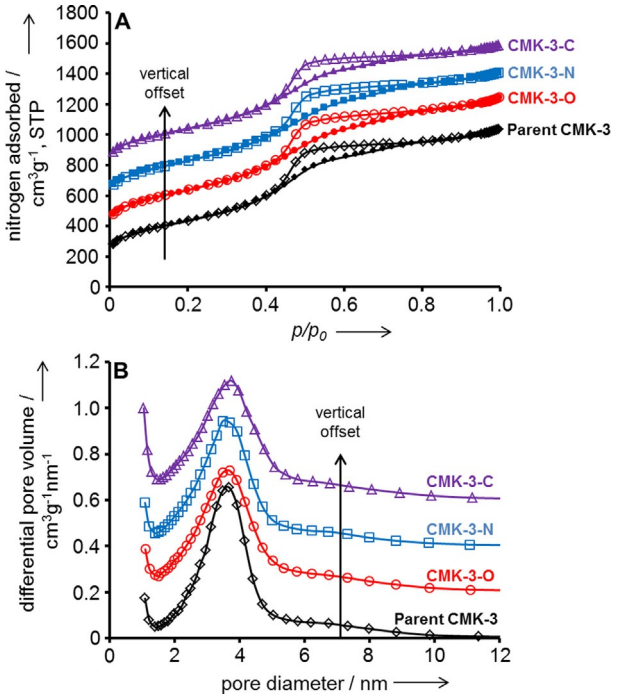

Figure 1. A) N_2 adsorption/desorption (filled symbols/empty symbols) isotherms (−196 °C) and B) differential pore size distributions of the parent CMK-3, CMK-3-O, CMK-3-N, and CMK-3-C. The volumes of N_2 adsorbed in A are offset vertically by 200, 400, and 600 $cm^3 g^{-1}$, and the differential pore volumes in B are offset vertically by 0.2, 0.4, and 0.6 $cm^3 g^{-1} nm^{-1}$ for CMK-3-0, CMK-3-N, and CMK-3-C, respectively.

Results and Discussion

Postsynthetic treatments of the parent CMK-3 material under a N_2 atmosphere at 900 °C and under air at 400 °C were performed to remove (CMK-3-C support) or introduce additional O-containing surface functional groups (CMK-3-O support), respectively. The additional exposure of the O-rich material to ammonia at 400 °C created N-containing groups on the support (CMK-3-N support). N_2 physisorption measurements (Figure 1 A) show that these treatments do not change the porosity of the carbon materials significantly. Independent of the functionalization treatment, the specific surface areas (SSAs) and total pore volumes (V_{Pore}) remain comparable to those of the parent CMK-3 (Table 1). All ordered mesoporous carbon materials provide specific surface areas in the range of 1500–1600 $m^2 g^{-1}$ and total pore volumes of 1.4–1.7 $cm^3 g^{-1}$. As already indicated by the comparable shape of the isotherms, the pore size distribution (PSD) and the average pore size of the functionalized materials also remain in the same range as those of the untreated material (Table 1 and Figure 1 B). All the functionalized supports retain a narrow PSD with sharp maxima in the narrow mesopore range (3.5–3.7 nm).

Surface analysis of the functionalized CMK-3 materials by using X-ray photoelectron spectroscopy (XPS; Table 2 and Figure S1) shows that the surface composition of the CMK-3 ma-

Table 1. Summary of the N_2 physisorption data of the parent CMK-3 material and the supports after different functionalization treatments and ICP-OES elemental analysis of the promoted and unpromoted catalysts after calcination.

Material	SSA [$m^2 g^{-1}$]	V_{Pore} [$cm^3 g^{-1}$]	$D_{Pore, Average}$ [nm]	Fe/Na/S (promoted) [wt%]	Fe/Na/S (unpromoted) [wt%]
Parent CMK-3	1543	1.55	3.8	–	–
CMK-3-O	1555	1.56	3.7	7.6/2.2/0.08	8.1/0.2/b.d.l.[a]
CMK-3-N	1530	1.62	3.5	7.1/2.3/0.08	7.6/0.2/b.d.l.
CMK-3-C	1555	1.45	3.6	7.1/2.2/0.07	7.9/0.2/b.d.l.

[a] b.d.l. = below detection limit.

Table 2. C, O, N, Fe, and Na surface atomic composition [at%] of the CMK-3 after different functionalization treatments and the promoted catalysts after calcination determined by using XPS analysis.

Material/catalyst	C	O	N	Fe	Na
CMK-3-O	90	9.9	0.2	0.0	0.0
CMK-3-N	91	5.7	3.5	0.0	0.0
CMK-3-C	98	2.2	0.0	0.0	0.0
Fe/Na/S-CMK-3-O	94	4.8	0.4	0.2	0.7
Fe/Na/S-CMK-3-N	86	9.2	2.9	0.4	1.3
Fe/Na/S-CMK-3-C	88	9.9	0.9	0.4	1.3

terials can be adjusted by the applied functionalization treatments. The surface oxygen content of CMK-3-C after the treatment under an inert atmosphere at 900 °C is only 2.2 at%, whereas that of CMK-3-O after heat treatment at 400 °C in air is 9.9 at%. The heating of the O-rich CMK-3 in ammonia at 400 °C leads to a decrease of the O content because of the partial substitution of the O-containing functional groups with N-containing groups. The fitting of the O 1s XPS spectra of the CMK-3 materials (Figures 2 A–C and Table S1) shows contributions of two major peaks located at binding energies (BEs) of 532–533 and 530–532 eV, which correspond to O–C or O=C, respectively.[30,35–38] Two peak shoulders with a lower intensity are located at BE ≈ 535 and 537 eV. The N 1s peaks of CMK-3-N are located at BE ≈ 398 and 399–400 eV, which correspond to pyridinic- and pyrrolic-type N species, respectively (Figure 2 D).[30,36] Furthermore, a minor peak is located at BE = 402–403 eV, which could originate from N–H bonds, oxidized N, or N incorporated into the graphite network.[28]

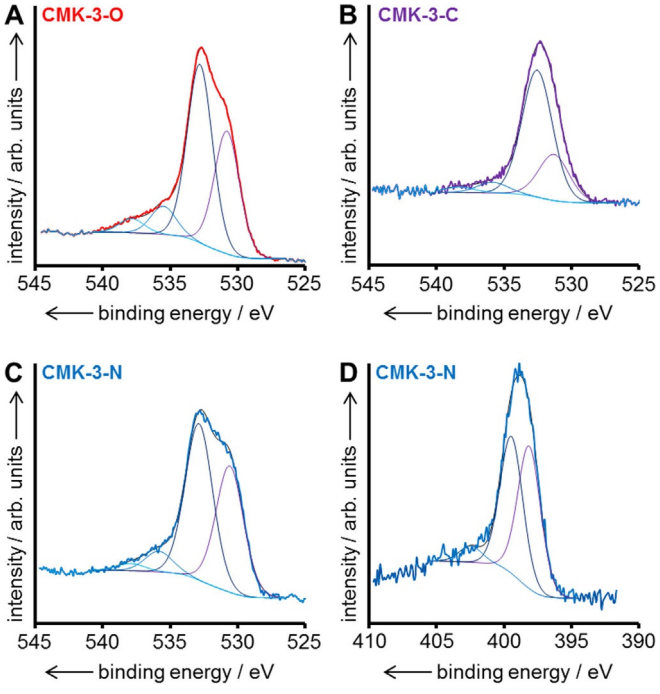

Figure 2. O 1s XPS spectra with fitted components of A) CMK-3-O, B) CMK-3-C, and C) CMK-3-N. D) N 1s XPS spectrum with fitted components of CMK-3-N.

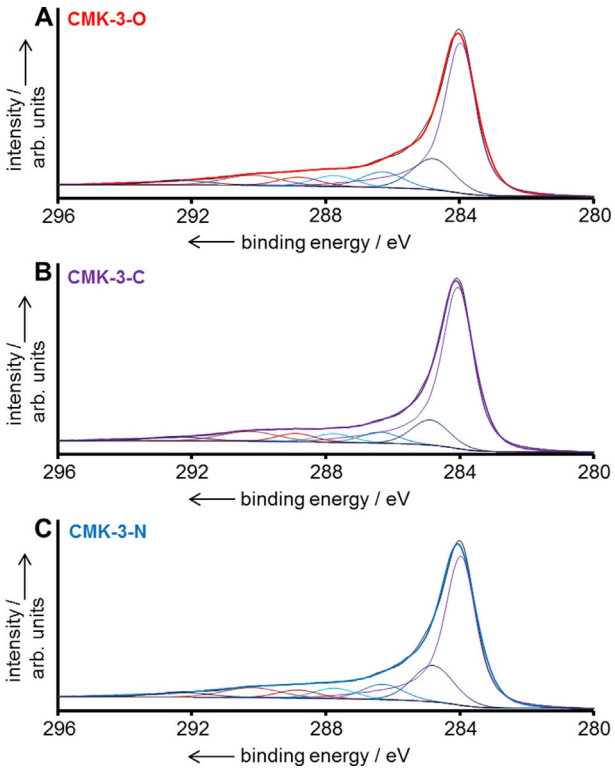

Figure 3. C 1s XPS spectra with fitted components of A) CMK-3-O, B) CMK-3-C, and C) CMK-3-N.

The C 1s XPS spectra of the CMK-3 materials can be deconvoluted into different components (Figure 3 and Table S2):[35,36] sp^2-hybridized graphitic surface C at BE ≈ 284.0 eV, sp^3-hybridized surface C species or defects in the graphitic framework at BE ≈ 284.8 eV, C–O (e.g., in phenols and ethers) at BE ≈ 286.3 eV, C=O (e.g., in ketones and quinones) at BE ≈ 287.5 eV, and O–C=O (e.g., in carboxyls and carboxylic anhydrides) at BE ≈ 288.8 eV. Furthermore, typical π–π* shakeup lines of graphite and graphitic-like compounds are present at BE ≈ 290.2 and 292.3 eV. The CMK-3-C material shows a smaller contribution of the sp^3-hybridized C species/defective graphite species at BE ≈ 284.8 eV (Table S2). The presence of functional surface groups leads to the formation of defects in the graphite-like nanostructure. Therefore, the carbon material with a lower degree of functionalization has a higher concentration of sp^2 surface C atoms. Notably, adsorbed volatile organic compounds from ambient air can also contribute to the peak at BE ≈ 284.8 eV.[39] The presence of minor concentrations of surface oxygen in CMK-3-C likely originates from the saturation of dangling bonds present after the thermal treatment at 900 °C upon the contact of the carbon material with ambient air.

Hydrogen thermogravimetric analysis (H_2-TGA) of the surface-modified CMK-3 materials provides further semiqualitative insights into the ratio of the functional groups (Figure S2). The CMK-3-C material shows the lowest weight loss of all the supports upon heating to 800 °C. As a result of the removal of surface functional groups present on the CMK-3 surface after synthesis, the residual mass of the heat-treated support material is significantly higher than that of the parent carbon material. In

contrast, the O-rich material shows a higher weight loss than the parent CMK-3 because of the presence of additional functional groups after heating in air. CMK-3-N shows a slightly higher residual mass and the weight loss starts at a higher temperature than that for CMK-3-O, likely related to the higher thermal stability of N-containing functional groups than O-containing groups.[40]

We used H_2-TGA coupled with mass spectrometry (MS) to show the release of H_2O as the decomposition product mainly at 340 and 400 °C, which originates from the removal of O-containing surface groups with a relatively low thermal stability (Figure S3 A). A significant peak at $m/z=18$ is present at ≈630 °C for CMK-3-O and CMK-3-N because of the release of O surface groups with a high stability that are not present in the CMK-3-C support. This is also observed for $m/z=17$, which corresponds to OH or NH_3 release (Figure S3 B). Further differences are observed in the CO_2 release ($m/z=44$) at ≈600 °C (Figure S3 C). The contribution of CO_2 release likely originates from carboxylic surface groups, carboxylic anhydrides, or lactones. No CO_2 release is detected in the CMK-3-C in accordance with the low contribution of doubly bound oxygen species at BE = 530–532 eV in the O 1s XPS spectra of this material (Figure 2 B and Table S1). The higher intensity of the CO_2 TGA peak of CMK-3-O than that of CMK-3-N suggests the presence of a higher concentration of carboxylic groups in the N-free material. The C 1s and O 1s XPS spectra show a comparable distribution of singly and doubly bound O species as well as carboxylic surface functional groups in CMK-3-O and CMK-3-N (Table S2). Hence, it can be concluded that (although no quantitative exchange occurs) there is no preferential substitution of a specific oxygen surface species by N and instead different kinds of groups are affected during the ammonia treatment.

Precursor salts of Fe and Fe with Na/S promoters were infiltrated into the CMK-3 pore system by incipient wetness impregnation (IWI) followed by drying and calcination at 400 °C under flowing N_2. TEM and high-angle annular dark-field scanning transmission electron microscopy (HAADF-STEM) images (Figure 4) of the calcined promoted catalysts show the presence of well-dispersed Fe nanoparticles with a size of 3–5 nm within the hexagonally ordered CMK-3 pore system. Energy-dispersive X-ray spectroscopy (EDX; Figure S4) and HAADF-STEM images of full CMK-3 particles (Figure S5) reveal the uniform distribution of Fe and the Na promoter over the entire support material. No large agglomerates are observed on the external surface area of the CMK-3 particles.

Inductively coupled plasma optical emission spectroscopy (ICP-OES; Table 1) was used to show that the composition of the catalysts can be controlled precisely by using the IWI technique. All calcined FTO catalysts have comparable Fe contents of 7.1–8.1 wt% Fe. In accordance with a previous study of Muhler et al. who used CNTs as supports,[29] different surface functionalization does not have a significant influence on the Fe loading capacities of the carbon materials. Na (2.2–2.3 wt%) and S (0.07–0.08 wt%) are present in the promoted catalysts. The unpromoted reference samples have much lower Na contents, and the amount of S is below the detection limit. Hence, any differences in the catalytic properties for the catalysts with different surface functional groups will not arise from unwanted variations in the Fe loadings or promoter contents.

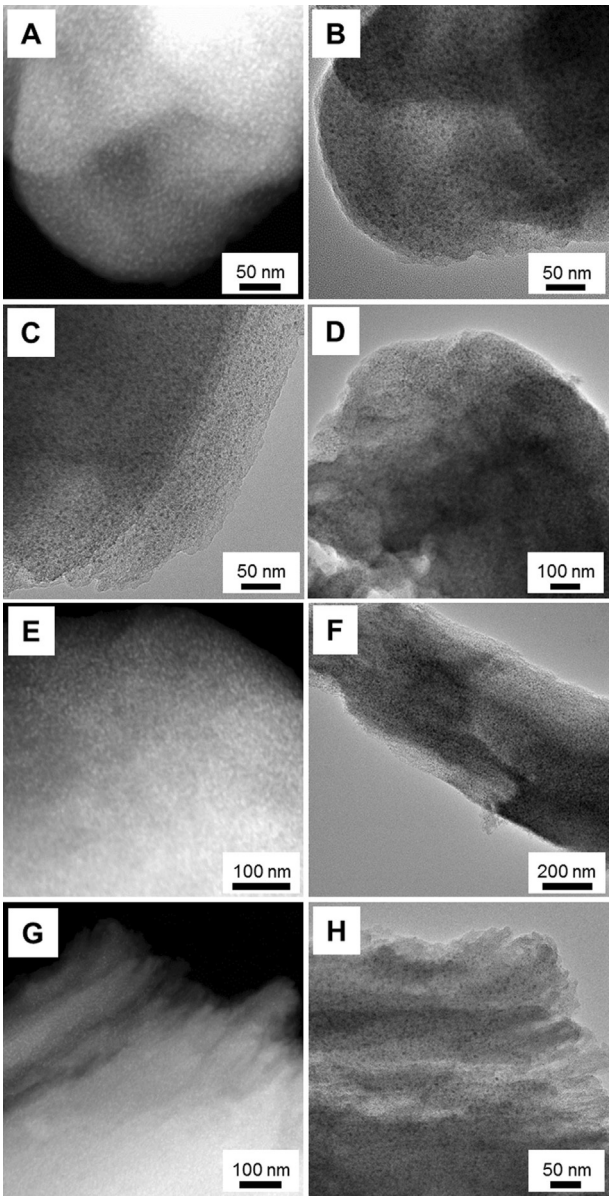

Figure 4. TEM and HAADF-STEM images of the calcined catalysts: A–C) Fe/Na/S-CMK-3-C, D–F) Fe/Na/S-CMK-3-O, and G, H) Fe/Na/S-CMK-3-N.

After calcination, a larger concentration of O surface species is present in the promoted Fe/Na/S-CMK-3-N and Fe/Na/S-CMK-3-C catalysts because of the presence of iron oxide particles (Table 2 and Figure S6). For instance, a significant amount of surface O (9.9 at%) is detected in the Fe/Na/S-CMK-3-C catalyst. The reaction of the decomposition products of the Fe and promoter salts with the CMK-3 surface and hence the formation of additional O groups on the support surface during calcination cannot be ruled out. The amount of surface Fe, O, and Na detected in the Fe/Na/S-CMK-3-O catalysts is significantly lower than that of Fe/Na/S-CMK-3-N and Fe/Na/S-CMK-3-C. Along with the higher surface sp^2-hybridized C content (Table S2), this indicates the more extensive encapsulation of

Fe particles within the mesopores of the carbon support after the calcination of this catalyst.

Interestingly, the amount of surface Fe determined by using XPS is much lower for all calcined catalysts than that determined by using ICP-OES on the bulk catalysts (Table 3). In contrast (with the exception of the Fe/Na/S-CMK-3-O), the detected amount of Na is comparable for both methods. This indicates that Na is distributed homogeneously over the surface of the CMK-3 particles, whereas Fe is largely encapsulated in the pore system of the carbon support.

Table 3. Comparison of the bulk (ICP-OES) and surface (XPS) Fe and Na elemental composition [wt%] of Fe/Na/S-CMK-3-N, Fe/Na/S-CMK-3-O, and Fe/Na/S-CMK-3-C after calcination.

Catalyst	$Fe_{ICP-OES}$	Fe_{XPS}	$Na_{ICP-OES}$	Na_{XPS}
Fe/Na/S-CMK-3-O	7.6	1.0	2.2	1.4
Fe/Na/S-CMK-3-N	7.1	1.7	2.3	2.3
Fe/Na/S-CMK-3-C	7.1	1.7	2.2	2.3

The C 1s XPS spectra of the calcined catalysts (Figure S7 and Table S2) show various different kinds of O-containing groups on the surface of the CMK-3-C support. In comparison to the spectra of the Fe-free support materials, it can be seen that the loading of Fe leads to an increase in the relative spectral contribution of the peak located at BE = 530–531 eV in the O 1s spectra that can be assigned to contributions from O anions in iron oxides (Figure S8 and Table S1).[30] Additional N-containing groups are also generated on the surface of the support, likely because of the decomposition of the ammonium iron citrate precursor. However, the surface N content of the Fe/Na/S-CMK-3-N catalyst is significantly higher than that of the CMK-3-C- and CMK-3-O-supported catalysts (Figure S8 and Table 2). Independent of the applied support material, the Fe 2p XPS spectra (Figure S9) show the characteristic shape for Fe^{3+} with two peaks at BE ≈ 711 (Fe $2p_{3/2}$) and 724 eV (Fe $2p_{1/2}$) with a shakeup satellite at BE ≈ 719 eV.[28]

Powder XRD measurements of the calcined catalysts (Figure S10) show that the Fe species are present in form of magnetite or hematite after calcination. This is in line with a previous Mössbauer spectroscopy study on CMK-3-supported Fe catalysts, which showed that Fe^{3+} is the dominant Fe species even after calcination at a slightly higher temperature.[15]

Hydrogen temperature-programmed reduction (H_2-TPR) analyses of the calcined promoted catalysts (Figure S11) show the typical multistep reduction profile of Fe_xO_y species as reported previously for CMK-3-supported Fe catalysts with a comparable composition.[15] The first peaks located at ≈350 °C originate from the formation of Fe_3O_4 from Fe_2O_3. The subsequent H_2 consumption at 450–500 °C is related to the reduction to FeO, and the formation of metallic Fe is observed at 600–700 °C. The inverse peaks observed at temperatures above 750 °C for the Fe/Na/S-CMK-3-N and Fe/Na/S-CMK-3-C catalysts could result from the methanation of the support that can occur in CMK-3-supported Fe catalysts after calcination, in particular, at calcination temperatures below 500 °C.[41] The Fe/Na/S-CMK-3-O catalyst shows a lower overall H_2 consumption and no methanation at higher temperatures. As shown recently, the formation of a carbon shell that surrounds the Fe particles can prevent the methanation of the carbon support by Fe even under H_2 at high temperatures.[41] However, quantitative information on FTO catalysts is difficult to extract from the H_2-TPR curves because of the overlapping contributions of Fe reduction and the release of surface groups during heating. A H_2-TPR analysis of the parent CMK-3 (Figure S11) shows that the release of surface functional groups leads to a noticeable contribution to the TPR profile over the whole relevant temperature range.

N_2 physisorption measurements of the calcined Fe/Na/S-CMK-3-O and Fe-Na/S-CMK-3-C catalysts (Figure S12 and Table S3) were used to show significant differences in their pore structures after Fe loading and calcination. The isotherm of Fe-Na/S-CMK-3-C still reveals the characteristic mesoporosity of the CMK-3-C support. In contrast, Fe/Na/S-CMK-3-O has a more microporous character with a higher micropore SSA but a lower total SSA and pore volume. This indicates the high reactivity of the O-functionalized support material during calcination and a stronger encapsulation of the Fe particles in this support, which is in line with the XPS and H_2-TPR data.

The catalytic properties of the Fe-based catalysts were investigated under industrially relevant FTO conditions at 10 bar, 340 °C, and $H_2/CO = 2$ (Figure 5 and Table S4). In general, Fe catalysts provide a high activity for the water gas shift reaction, and hence CO-rich syngas (e.g., syngas obtained from coal or biomass) can be applied directly without the prior adjustment of its composition. In our experiments, in line with industrial practice, we apply $H_2/CO = 2$ to avoid excessive coke formation and unwanted pressure increases in the FTO experiments. The catalyst supported on the O-enriched CMK-3 and the support with a higher N content show the lowest catalytic activity in the absence of promoters (Figure 5 A). Only the Fe-CMK-3-C catalyst maintains a noticeable iron time yield (FTY) with time on stream (TOS) in the absence of Na and S. The generally low catalytic activity of these catalysts might be because of the absence of Na/S promoters, the restricted accessibility of the Fe particles encapsulated within the narrow pore system of CMK-3, and limited iron carbide formation. A recent study has shown that the activity of unpromoted catalysts depends strongly on the degree of carbidization of the Fe.[33]

Independent of the surface properties of the support, the promoted catalysts show a higher initial activity (CO conversions of ≈20%) and a higher Fe-weight-based activity, likely because of enhanced iron carbidization. A recent study on carbon-nanofiber-supported FTO catalysts has shown that the formation of iron carbide is significantly more rapid in the presence of Na and S promoters, which leads to a higher initial catalytic activity.[33] After an initial decrease of the CO conversion, all promoted CMK-3-supported catalysts show a slight increase of the catalytic activity followed by stable operation for up to 120 h TOS. However, the enhancement of the activity compared to that of the unpromoted catalysts is more significant for Fe/Na/S-CMK-3-N and Fe/Na/S-CMK-3-C than for Fe/Na/S-CMK-3-O. Comparable trends have been reported by

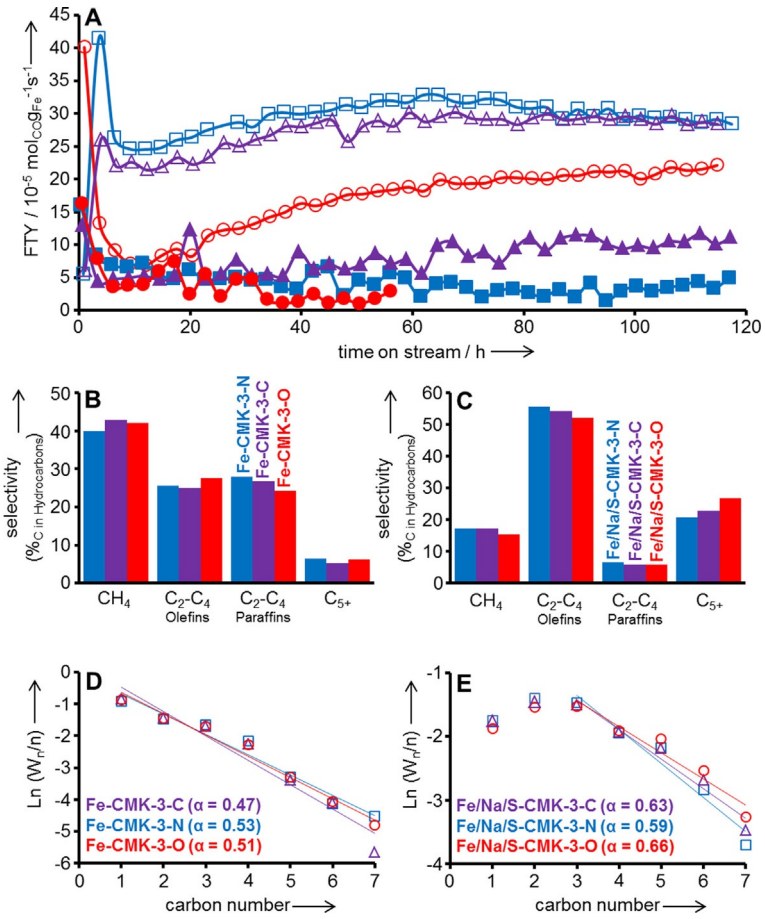

Figure 5. A) FTY against TOS of the Na/S-promoted (empty symbols) and unpromoted (filled symbols) Fe-based FTO catalysts supported on CMK-3-O, CMK-3-N, and CMK-3-C. B, C) Hydrocarbon product selectivity and D, E) the corresponding ASF plots of the C_1–C_7 product fractions of unpromoted and promoted catalysts, respectively. The chain growth probability (α) is calculated from the C_3–C_7 and C_1–C_7 products for the promoted und unpromoted catalysts, respectively. Data obtained at $H_2/CO = 2$, $T = 340\,^{\circ}C$, $p = 10$ bar, TOS ≈ 100 h (promoted catalysts) or 0–4 h (unpromoted catalysts).

Chew et al. without promoters for O-functionalized CNTs, which showed a lower catalytic activity than N-functionalized CNTs and O-functionalized CNTs treated under an inert atmosphere.[30] This was attributed to the lower thermal stability of O-containing surface groups and the carbon encapsulation of the Fe particles in the former. This is in line with the XPS and N_2 physisorption analysis results of the calcined Fe/Na/S-CMK-3-O catalyst, which showed lower Fe and higher C surface concentrations as well as stronger encapsulation and, therefore, provides a lower number of catalytically active sites.

The promoted catalysts show a lower methane formation, a higher selectivity for C_2–C_4 olefins, and a higher chain growth probability than the unpromoted catalysts (Figure 5 B–E). However, the selectivity values might not be compared easily because of the different CO conversions in the presence and absence of Na/S (Table S4). The difference in the selectivity between the promoted catalysts on different supports is not significant. However, Fe/Na/S-CMK-3-N shows the highest selectivity to C_2–C_4 olefins in the hydrocarbon products of 55 %$_C$ after 100 h TOS (Figure 5 C). Similar findings were reported for N-functionalized CNT supports.[30] All catalysts show methane and C_2 formation below the predictions of the Anderson–Schulz–Flory (ASF) model (Figure 5 E), which indicates the efficiency of the promoters under industrially relevant conditions. The CO_2 selectivities of the promoted catalysts are 40–50 %$_C$.

In agreement with a previous study on promoted CMK-3-supported FTO catalysts, TEM investigations of the spent promoted catalysts show a growth of the Fe particles to 18–26 nm in size (Figure 6).[15] The confinement of the particles in the pore system of CMK-3 with different surface functionalization can slow but not fully prevent particle growth during catalyst operation under industrially relevant conditions. The growth rate of the particles is related to their catalytic activity as the highest growth rate is observed for the Fe/Na/S-CMK-3-N catalyst, which has the highest catalytic activity, whereas the Fe/Na/S-CMK-3-O and Fe/Na/S-CMK-3-C catalysts have smaller Fe particles after 120 h TOS. However, from the comparable activity but slightly larger Fe particle size of the Fe/Na/S-CMK-3-N catalyst compared to Fe/Na/S-CMK-3-C after 120 h of TOS we can conclude that the additional presence of N-containing groups on the surface of the carbon support can increase the catalytic activity of Fe-based FTO catalysts on CMK-3 supports.

Notably, after calcination, a high concentration of O-containing surface groups is also present in the Fe/Na/S-CMK-3-C catalyst but this catalyst contains a larger concentration of surface Fe than Fe/Na/S-CMK-3-O. In view of the similar Fe particle size

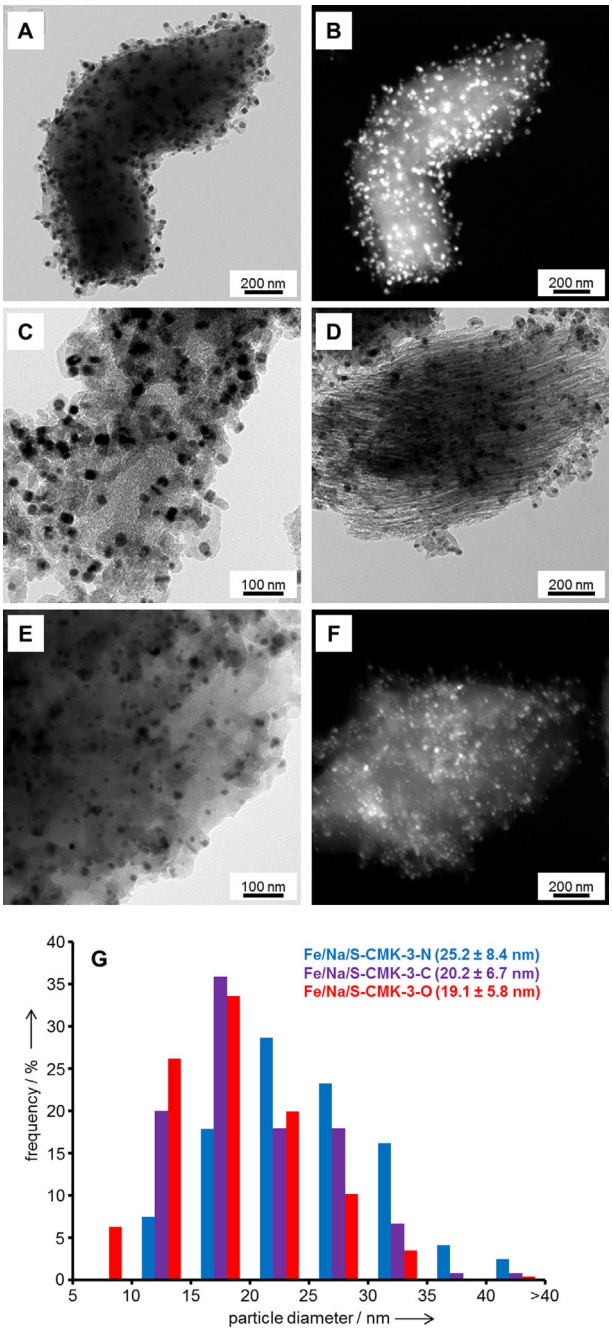

Figure 6. TEM and HAADF-STEM images of the spent promoted catalysts A, B) Fe/Na/S-CMK-3-C, C) Fe/Na/S-CMK-3-N, and D–F) Fe/Na/S-CMK-3-O and G) the corresponding Fe particle size distributions after ≈120 h of TOS under industrially relevant FTO conditions (H_2/CO = 2, T = 340 °C, p = 10 bar).

of the spent catalysts, the higher catalytic activity is related to structural effects that occur during the calcination of the catalysts in combination with the influence of the surface groups during catalysis.

Conclusions

The surface of ordered mesoporous CMK-3 carbon materials can be modified by different postsynthetic treatments. Heating in air atmosphere at 400 °C results in a surface oxygen content of 9.9 at%, whereas heating in N_2 leads to a lower surface O concentration of 2.2 at%. Ammonia treatment of the O-functionalized material removes oxygen species partially and introduces up to 3.5 at% of surface N. After the infiltration of Fe and Na and S promoters, uniformly distributed metal particles are encapsulated in the pore system of the CMK-3 samples with a comparable size independent of the surface properties.

Under industrially relevant Fischer–Tropsch to olefins (FTO) conditions, the addition of promoters leads to a more significant enhancement of the activity than surface functionalization alone. The activity of the FTO catalysts supported on N-doped CMK-3-N and the thermally treated CMK-3-C support is higher than that of the O-rich CMK-3-O support at a comparable particle size. Our findings indicate that the O-functionalization of the carbon supports leads to a lower catalytic activity than N-enrichment or thermal treatment, likely because of the very strong encapsulation of Fe particles with the carbon during calcination, which blocks the catalytically active sites. In general, the effect of the surface properties of the support on the selectivity of the catalysts remains low. Methane formation can be suppressed by the addition of Na and S promoters for all support surfaces. Surface functionalization does thus not have drastic effects on the efficiency of the Na and S promoters. The presence of N-containing groups leads to a slight improvement of the catalytic activity and a lower olefin production in the presence of promoters. Hence, a combination of promoters and the N-functionalization of CMK-3 supports is a useful method to enhance the activity of Fe-based FTO catalysts and retain a high selectivity to C_2–C_4 olefins and the low methane production provided by the promoters.

Experimental Section

Synthesis and surface functionalization of CMK-3: CMK-3 carbon material with a hexagonal mesopore arrangement was synthesized by mixing SBA-15 silica (2 g, treated hydrothermally at 130 °C) with a solution of sucrose (2.5 g) and concentrated H_2SO_4 (280 mg) in H_2O (10 mL) in a porcelain dish. The carbohydrate was polymerized by heating the mixture to 100 °C for 6 h and to 160 °C for another 6 h in air. Subsequently, impregnation was repeated with a solution of sucrose (1.6 g) and concentrated H_2SO_4 (180 mg) in H_2O (10 mL), again followed by heating again to 100 and 160 °C. Carbonization was performed in a tubular furnace under constant N_2 flow at 900 °C for 2 h with a heating rate of 150 °C h^{-1}. SBA-15 dissolution was achieved by treating the carbon/SBA-15 composite material in a mixture of hydrofluoric acid (concentrated solution in H_2O)/H_2O/EtOH (1:1:1 by volume, ≈125 mL) in a closed polypropylene bottle overnight followed by filtration, washing with ethanol, and drying at RT. The CMK-3 yield was ≈1.1 g.

CMK-3 with a large number of O-containing surface groups (CMK-3-O) was synthesized by placing the as-made parent material in a porcelain dish followed by heat treatment in a muffle furnace under static air atmosphere at 400 °C for 1 h with a heating rate of 100 °C h^{-1}. CMK-3 with N-containing surface functional groups (CMK-3-N) was synthesized by treatment of the CMK-3-O at 400 °C for 6 h under an NH_3 flow of 25 mL min^{-1} in a quartz glass cell followed by cooling to RT under a He flow of 25 mL min^{-1}. CMK-3 with low amount of surface functional groups (CMK-3-C) was synthesized by heat treatment of the parent CMK-3 in a tubular fur-

nace under a N_2 flow for 2 h at 900 °C at a heating rate of 100 °C h^{-1}.

Synthesis of FTO catalysts: In a mortar, the surface-functionalized CMK-3 supports (135 mg) were impregnated slowly with an aqueous solution (≈250 μL) of ammonium iron(III) citrate (94 mg, Fluka, 14.5–16% Fe), sodium citrate dihydrate (19 mg, 99%, Sigma Aldrich), and iron(II) sulfate heptahydrate (1.3 mg, 99%, Sigma Aldrich). In the case of the nonpromoted catalysts, no sodium citrate or iron sulfate was added to the impregnation solution. The impregnated sample was dried at 120 °C under static air over night. Calcination was performed for 2 h at 400 °C in a tubular furnace in N_2 flow with a heating rate of 2 °C min^{-1}. The different catalysts are labeled as "Fe-Support" (unpromoted) or "Fe/Na/S-Support" (promoted).

Catalyst characterization: N_2 physisorption isotherms were measured at −196 °C by using a Micromeritics TriStar 3000 instrument. Before the measurements, samples were dried at 150 °C under flowing N_2. SSAs were calculated using the multipoint BET method ($0.05 < p/p_0 < 0.25$). V_{Pore}, PSDs, and average pore diameters ($D_{Pore,Average}$) were determined by the Barrett–Joyner–Halenda (BJH) method by using the adsorption branches of the isotherms.

ICP-OES was performed by using a SPECTRO ARCOS ICP-OES instrument after aqua regia extraction of the samples.

H_2-TPR was performed by heating ≈40 mg of the calcined catalysts up to 1000 °C at a rate of 5 °C min^{-1} in 50 mL min^{-1} of a gas mixture of 5% H_2 in Ar by using a Micromeritics Autochem II 2920 Chemisorption Analyzer.

H_2-TGA of the calcined catalysts was performed by using a PerkinElmer Pyris1TGA instrument. Samples were heated from RT to 800 °C at a rate of 5 °C min^{-1} in 50 mL min^{-1} of a gas mixture of 20% H_2 in Ar. MS was performed by using an Omnistar MS instrument from Pfeiffer Vacuum Benelux BV.

XRD measurements were performed by using a Bruker D2 PHASER with a $CoK_{\alpha 1}$ radiation source ($\lambda = 0.1788$ nm).

XPS was performed by using a Thermo Scientific K-Alpha spectrometer equipped with a monochromatic small-spot X-ray source and a 180° double focusing hemispherical analyzer with a 128-channel delay line detector. Spectra were obtained using an aluminum anode ($AlK_\alpha = 1486.6$ eV) operated at 72 W and a spot size of 400 μm. Survey scans were measured at constant pass energy of 200 eV, and high-resolution scans of the separate regions were measured at 50 eV. The background pressure of the ultra-high vacuum (UHV) chamber was 2×10^{-8} mbar. No special precautions were taken to keep the sample under an inert atmosphere during catalyst transfer and handling. Sample charging was compensated for by the use of an electron flood gun, and binding energy calibration was done by setting the peak of graphitic sp^2 carbon to BE = 284.0 eV.

TEM, HAADF-STEM, and EDX of the calcined analysis were performed by using a FEI Talos F200X transmission electron microscope operated at 200 kV and equipped with a high-brightness field emission gun (X-FEG) and a Super-X G2 EDX detector. TEM and HAADF-STEM analysis of the spent catalysts were performed by using an FEI Tecnai 20 FEG instrument operated at 200 kV. Before the measurements, the samples were ground into fine powders, dispersed in ethanol, sonicated for ≈30 s, and drop-casted on a carbon-coated copper TEM grid.

Catalyst testing: The FTO catalysts were tested under industrially relevant conditions by using a 16-reactor catalytic testing setup (Flowrence, Avantium) at 10 bar, 340 °C, and a H_2/CO ratio of 2 (by volume). The FTO reaction was performed at medium CO conversions (≈20% initial conversion). Calcined catalysts were sieved to a particle size fraction of 38–90 μm. The unpromoted catalyst (4–6 mg) and the promoted catalyst (10–13 mg) were diluted with silicon carbide (50 μL, 212–425 μm) and transferred to a tubular fixed-bed reactor. The catalysts were dried in a He flow at 280 °C for 20 min at 3 bar followed by subsequent change to a flow of H_2/CO (2:1 by volume) at 280 °C and 3 bar for 10 min. Then, the temperature was increased to 340 °C (heating rate = 2 °C min^{-1}) and after 10 min the pressure was increased to 10 bar (TOS = 0 h). The gas hourly space velocity (GHSV) was in the range of 10000–30000 h^{-1}. The products were analyzed by using online GC (Agilent 7890A). The permanent gases and CO_2 were separated on a ShinCarbon ST column and quantified against He as an internal standard using a thermal conductivity detector (TCD). CO conversions were calculated as $X_{CO} = (mol_{CO,in} - mol_{CO,out})/mol_{CO,in}$. Hydrocarbons ($C_1$–$C_9$) were separated on an Agilent J&W PoraBOND Q column, detected using an flame ionization detector (FID) and quantified against the TCD signal of the internal standard He. The activity of the catalysts is expressed as FTY in moles of converted CO per gram of Fe per second. The product selectivity [$\%_{Carbon}$] was calculated as the equivalent of carbon atoms present in a product fraction in relation to total carbon atoms present in the formed hydrocarbons. At the end of the catalytic testing experiment, the reactors were cooled to RT under a flow of He.

Acknowledgements

M.O. acknowledges financial support provided by the German academic exchange service (Deutscher Akademischer Austauschdienst, DAAD). K.P.d.J. gratefully acknowledges funding from the European Research Council, EU FP7 ERC Advanced Grant no. 338846. We thank Helen de Waard (Utrecht University, Faculty of Geosciences) for the ICP-OES measurements. M. W. G. M. (Tiny) Verhoeven of Eindhoven University of Technology is thanked for assistance in XPS measurements and analysis. We further thank Anja Werner and Prof. Stefan Kaskel (TU Dresden, Inorganic Chemistry) for help with the ammonia treatment of the samples.

Keywords: carbon · iron · surface chemistry · mesoporous materials · supported catalysts

[1] A. Corma, F. V. Melo, L. Sauvanaud, F. Ortega, *Catal. Today* **2005**, *107–08*, 699–706.
[2] H. M. Torres Galvis, K. P. de Jong, *ACS Catal.* **2013**, *3*, 2130–2149.
[3] Q. Zhang, J. Kang, Y. Wang, *ChemCatChem* **2010**, *2*, 1030–1058.
[4] M. Janardanarao, *Ind. Eng. Chem. Res.* **1990**, *29*, 1735–1753.
[5] U. Olsbye, S. Svelle, M. Bjrgen, P. Beato, T. V. W. Janssens, F. Joensen, S. Bordiga, K. P. Lillerud, *Angew. Chem. Int. Ed.* **2012**, *51*, 5810–5831; *Angew. Chem.* **2012**, *124*, 5910–5933.
[6] G. Cai, Z. Liu, R. Shi, H. Changqing, L. Yang, C. Sun, Y. Chang, *Appl. Catal. A* **1995**, *125*, 29–38.
[7] F. Jiao, J. Li, X. Pan, H. Li, M. Wei, Y. Pan, Z. Zhou, M. Li, S. Miao, J. Li, Y. Zhu, D. Xiao, T. He, J. Yang, F. Qi, Q. Fu, X. Bao, *Science* **2016**, *351*, 1065–1068.
[8] K. Cheng, B. Gu, X. Liu, J. Kang, Q. Zhang, Y. Wang, *Angew. Chem. Int. Ed.* **2016**, *55*, 4725–4728; *Angew. Chem.* **2016**, *128*, 4803–4806.

[9] H. M. Torres Galvis, J. H. Bitter, C. B. Khare, M. Ruitenbeek, A. I. Dugulan, K. P. de Jong, *Science* **2012**, *335*, 835 – 838.
[10] E. Iglesia, *Appl. Catal. A* **1997**, *161*, 59 – 78.
[11] A. Y. Khodakov, W. Chu, P. Fongarland, *Chem. Rev.* **2007**, *107*, 1692 – 1744.
[12] S. Abelló, D. Montané, *ChemSusChem* **2011**, *4*, 1538 – 1556.
[13] C. López, A. Corma, *ChemCatChem* **2012**, *4*, 751 – 752.
[14] V. R. R. Pendyala, U. M. Graham, G. Jacobs, H. H. Hamdeh, B. H. Davis, *ChemCatChem* **2014**, *6*, 1952 – 1960.
[15] M. Oschatz, W. S. Lamme, J. Xie, A. I. Dugulan, K. P. de Jong, *ChemCatChem* **2016**, *8*, 2846 – 2852.
[16] H. M. Torres Galvis, A. C. J. Koeken, J. H. Bitter, T. Davidian, M. Ruitenbeek, A. I. Dugulan, K. P. De Jong, *Catal. Today* **2013**, *215*, 95 – 102.
[17] J. Xie, J. Yang, A. I. Dugulan, A. Holmen, D. Chen, K. P. de Jong, M. J. Louwerse, *ACS Catal.* **2016**, *6*, 3147 – 3157.
[18] X. Zhou, J. Ji, D. Wang, X. Duan, G. Qian, D. Chen, X. Zhou, *Chem. Commun.* **2015**, *51*, 8853 – 8856.
[19] K. Cheng, M. Virginie, V. V. Ordomsky, C. Cordier, P. A. Chernavskii, M. I. Ivantsov, S. Paul, Y. Wang, A. Y. Khodakov, *J. Catal.* **2015**, *328*, 139 – 150.
[20] K. Cheng, V. V. Ordomsky, B. Legras, M. Virginie, S. Paul, Y. Wang, A. Y. Khodakov, *Appl. Catal. A* **2015**, *502*, 204 – 214.
[21] B. Sun, K. Xu, L. Nguyen, M. Qiao, F. F. Tao, *ChemCatChem* **2012**, *4*, 1498 – 1511.
[22] Y. Cheng, J. Lin, K. Xu, H. Wang, X. Yao, Y. Pei, S. Yan, M. Qiao, B. Zong, *ACS Catal.* **2016**, *6*, 389 – 399.
[23] C. Wang, P. Zhai, Z. Zhang, Y. Zhou, J. Ju, Z. Shi, D. Ma, R. P. S. Han, F. Huang, *Part. Part. Syst. Charact.* **2015**, *32*, 29 – 34.
[24] J. Tu, M. Ding, Q. Zhang, Y. Zhang, C. Wang, T. Wang, L. Ma, X. Li, *ChemCatChem* **2015**, *7*, 2323 – 2327.
[25] V. P. Santos, T. A. Wezendonk, J. J. D. Jaén, A. I. Dugulan, M. A. Nasalevich, H.-U. Islam, A. Chojecki, S. Sartipi, X. Sun, A. A. Hakeem, A. C. J. Koeken, M. Ruitenbeek, T. Davidian, G. R. Meima, G. Sankar, F. Kapteijn, M. Makkee, J. Gascon, *Nat. Commun.* **2015**, *6*, 6451.
[26] H. Xiong, L. L. Jewell, N. J. Coville, *ACS Catal.* **2015**, *5*, 2640 – 2658.
[27] D. S. Su, S. Perathoner, G. Centi, *Chem. Rev.* **2013**, *113*, 5782 – 5816.
[28] J. Lu, L. Yang, B. Xu, Q. Wu, D. Zhang, S. Yuan, Y. Zhai, X. Wang, Y. Fan, Z. Hu, *ACS Catal.* **2014**, *4*, 613 – 621.
[29] H. J. Schulte, B. Graf, W. Xia, M. Muhler, *ChemCatChem* **2012**, *4*, 350 – 355.
[30] L. M. Chew, W. Xia, H. Düdder, P. Weide, H. Ruland, M. Muhler, *Catal. Today* **2016**, *270*, 85 – 92.
[31] M. D. Sánchez, P. Chen, T. Reinecke, M. Muhler, W. Xia, *ChemCatChem* **2012**, *4*, 1997 – 2004.
[32] X. Chen, D. Deng, X. Pan, Y. Hu, X. Bao, *Chem. Commun.* **2015**, *51*, 217 – 220.
[33] J. Xie, H. M. T. Galvis, A. C. J. Koeken, A. Kirilin, A. I. Dugulan, M. Ruitenbeek, K. P. de Jong, *ACS Catal.* **2016**, *6*, 4017 – 4024.
[34] J.-S. Lee, S. H. Joo, R. Ryoo, *J. Am. Chem. Soc.* **2002**, *124*, 1156 – 1157.
[35] S. Kundu, Y. Wang, W. Xia, M. Muhler, *J. Phys. Chem. C* **2008**, *112*, 16869 – 16878.
[36] R. Arrigo, M. Hävecker, S. Wrabetz, R. Blume, M. Lerch, J. McGregor, E. P. J. Parrott, J. A. Zeitler, L. F. Gladden, A. Knop-Gericke, R. Schlögl, D. S. Su, *J. Am. Chem. Soc.* **2010**, *132*, 9616 – 9630.
[37] S. Reiche, R. Blume, X. C. Zhao, D. Su, E. Kunkes, M. Behrens, R. Schlögl, *Carbon* **2014**, *77*, 175 – 183.
[38] R. Schlögl, G. Loose, M. Wesemann, *Solid State Ionics* **1990**, *43*, 183 – 192.
[39] D. J. Miller, M. C. Biesinger, N. S. McIntyre, *Surf. Interface Anal.* **2002**, *33*, 299 – 305.
[40] W. Xia, *Catal. Sci. Technol.* **2016**, *6*, 630 – 644.
[41] M. Oschatz, T. W. van Deelen, J. L. Weber, W. S. Lamme, G. Wang, B. Goderis, O. Verkinderen, A. I. Dugulan, K. P. de Jong, *Catal. Sci. Technol.*, **2016**, DOI: 10.1039/C6CY01251E.

Manuscript received: September 30, 2016
Revised: November 10, 2016
Accepted Article published: November 16, 2016
Final Article published: January 18, 2017

